Dynamic NMR Imaging of Rapid Depth Filtration of Clay in Porous Media

E. J. Fordham, T. P. L. Roberts, T. A. Carpenter, and L. D. Hall
Herchel Smith Laboratory for Medicinal Chemistry, Cambridge University School of Clinical Medicine, Cambridge CB2 2PZ England

C. Hall
Schlumberger Cambridge Research Ltd., Cambridge CB3 0HG, England

The transport of particulate fluid suspensions through porous media and the subsequent clogging of the medium by internal or "depth" filtration is of interest in several petroleum and process engineering contexts, including both oil-well drilling and reservoir management. In drilling, the clogging of porous rock under the drill bit by particulates from the drilling fluid, over timescales comparable to cutter periods, influences drilling performance through its effect on pore pressure fields near the bit (Peltier and Atkinson, 1987; Fordham et al., 1991). Experimental techniques to observe such transport and clogging dynamically on timescales of seconds have not hitherto been available, although classical studies of total filtrate volume outflow are known (Darley, 1965). We report here dynamic observations of clay particle transport and clogging in the pores of a natural sedimentary rock, using a novel NMR (nuclear magnetic resonance) imaging technique, "prefocused FLASH" (Roberts et al., 1990), whereby T_1-weighted images of 128×64 pixels are acquired in about 1.9 s. Short movie loops of clay transport and clogging on a timescale of the order of 10 s have thereby been acquired. The technique is applied for the first time to porous media and may be of interest in analogous filtration contexts in chemical technology.

Experimental Studies

Experiments were performed in a small pressure cell manufactured from polyacetal. The cell holds 37-mm-long, 26-mm-dia. rock cores, sealed over their curved surfaces with a moulded rubber sleeve pressurized externally with compressed air at 0.6 MPa. Rock specimens were vacuum-saturated with deaerated deionized water before mounting. A sintered PTFE frit collects filtrate for drainage from the lower end and the cell was loaded above with a particulate suspension. The whole cell was mounted inside a split-ring resonator (Hall et al., 1985) of 65 mm ID. For our first investigations, the combination of natural porous medium of unusually large pore size with a suspension of finely divided swelling clay was used. The rock specimens were Ketton stone from the Peterborough area of England. "The classic oolitic limestone" (Leary, 1983), it has a porosity of about 0.25, dominant grain sizes of the order of 300 μm as revealed by scanning electron microscopy, dominant pore throat sizes of the order of 40 μm as determined by mercury porosimetry, and a hydraulic permeability of the order of 10 μm^2, which is exceptionally high for competent natural rocks. The clay mud was a water-based suspension of a commercial oilfield bentonite, predominantly sodium montmorillonite. The clay platelets may be as thin as 1 nm, with lateral dimensions of a few micrometers. The volume fraction of solids in the suspension was above 0.027. The cell was loaded with the rock and the clay mud, pressurized above 0.13 MPa with an initial step change imposed by a solenoid valve. Imaging was performed repeatedly for a period of 2 minutes with the pressure applied some 10 seconds into the procedure. NMR data were acquired using an Oxford Instruments 31-cm-bore magnet and an Oxford Research Systems Biospec I console operating at 83.7 MHz for proton resonances. Home-made 20-cm-ID gradient coils were used giving maximum field gradient strengths of 35 $mT \cdot m^{-1}$.

NMR Imaging Method

The NMR protocol involved a sequence of shaped radio-frequency pulses, which perform slice-selective excitation in the presence of a linear field gradient and collection of gradient recalled echoes (Haase et al., 1986). In-plane spatial encoding is achieved in the standard Fourier imaging manner, by frequency-encoding in one direction and by phase encoding in the other (see, for example, Morris, 1986). The pulses were designed using simulated annealing (Kirkpatrick et al., 1983) to achieve sharply defined band-selective excitation with minimal phase dispersion (Roberts et al., 1990; Hall et al., 1990). Such "prefocused" pulses with the excited spins in phase immediately after the pulse were achieved by allowing them to

E. J. Fordham is on leave from Schlumberger Cambridge Research Ltd.

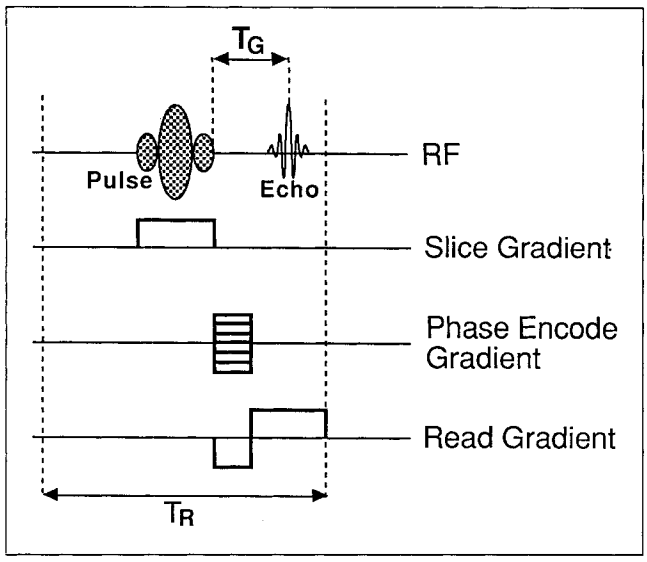

Figure 1. "Prefocused FLASH" pulse sequence.

The representation of the pulse is symbolic only; the pulse is highly complex and asymmetric. The displayed sequence is repeated for the chosen number of phase encode increments, 64 in our examples. No additional signal averaging is employed. Pulse length and gradient magnitudes determine the thickness of the slice selected by the pulse.

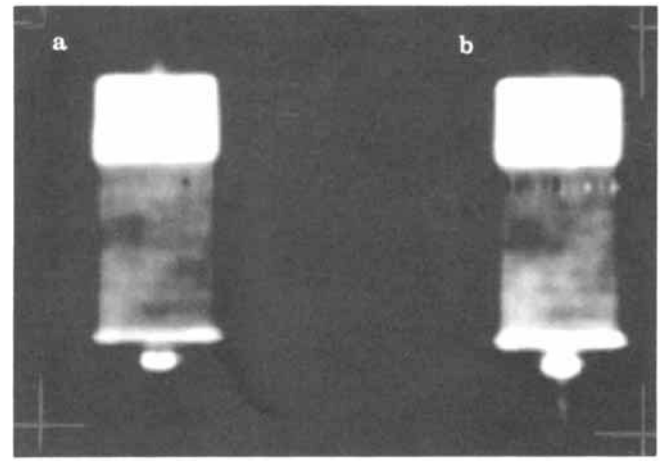

Figure 2. (a) Standard spin-warp (128^2 pixel) image of a 0.5-cm slice through the loaded pressure cell; (b) the same after the filtration process.

Echo time T_E was 11 ms and gradient strengths were approximately 9 m T·m^{-1}. High signal intensity is observed from the loading of clay suspension above and from the water-saturated frit below. Mud- or water-filled tube fittings are also shown above and below, demonstrating the centrality of the selected slice. Some structure is visible in the rock (superficially homogeneous) even at this slice thickness. The "waisted" appearance of the rock is a genuine feature of the geometry.

be time-asymmetric amplitude- and phase-modulated. This gives them the additional feature that any transverse magnetization in existence prior to their application is "spoiled" or dephased by the pulse (Roberts et al., 1991). Each echo collected, therefore, contains signal arising only from those spins that had recovered to equilibrium in the time T_R since the previous pulse. Hence, the signal is T_1-weighted. This "spoiler" property of the "prefocused" pulses is important in this technique; to obtain true T_1-weighting with simpler band-selective pulses requires additional spoiler gradients to suppress spurious echo signals (Frahm et al., 1987; Roberts et al., 1991). The T_1-weighting allows us to identify clay migration into the rock, because of well-known influence of surface to volume ratio on T_1 (Fripiat et al.,1982).

Figure 1 shows the repeat unit of the "prefocused FLASH" sequence. The time required to acquire an image is the product of the repeat unit length T_R and the number of pixels in the second imaging dimension (the "phase-encode" direction). Unlike conventional NMR spin-echo imaging, it is not necessary to wait for complete longitudinal relaxation between pulses (usually $\sim 5T_1$), and so T_R may be of the order of tens of ms, rather than several seconds. This is the basis of the rapid imaging facility. The gradient-recalled echoes used also help to keep the pulse sequence short; however, because no refocusing pulses are used, the applicability of the technique is restricted by the T_2^* (the effective transverse relaxation time constant) of the specimen rather than its T_2 (the intrinsic transverse relaxation time constant). Nevertheless, successful images were obtained with rock specimens of natural linewidths (full width at half maximum) of 380 Hz at the field strength used, corresponding to a T_2^* of about 1 ms. For the slice thickness of 10 mm, a 5-ms-long pulse ($\sim 5T_2^*$) was used; and the success of the method on such specimens depends on a further property that total transverse magnetization remains small until late in the pulse. This will be the subject of a future publication. A simple model for the signal weighting $S(y; T_R, T_G)$, assuming single exponential relaxation, would be:

$$S(y; T_R, T_G) \propto \rho(y) \times \{1 - \exp[-T_R/T_1(y)]\} \exp[-T_G/T_2^*(y)] \quad (1)$$

where y is the vertical image co-ordinate, $\rho(y)$ is the vertical profile of proton density, and T_G is the gradient echo time (Figure 1). Relaxation processes in porous media are well-known to be multi-exponential, but Eq. 1 suffices for qualitative discussion of image intensity variations.

Results and Interpretation

A standard spin-warp image (Edelstein et al., 1980) of the cell before filtration is shown in Figure 2a, where all major internal features of the pressure cell can be seen. There was no major change in a similar image (Figure 2b) after filtration although changes in T_2 within the rock on invasion by clay-bearing fluid reduce rock water signal levels somewhat relative to the uninvaded rock.

A sequence of "prefocused FLASH" images is shown in Figure 3. At the T_R used (29 ms), little internal structure is visible in the rock (Figure 3a, $t = 7.6$ s), although different thresholding does reveal signal. This is expected; and the rock has an uninvaded T_1 of the order of 1.2 s ($40T_R$). The water-soaked frit is dim for the same reason, although it is brighter than the rock because of its higher porosity (and probably greater T_2^*). Increasing the T_R to 120 ms or greater begins to reveal greater structure in the rock, even with the considerable "pedestal" of signal arising from the mud reservoir, but at the expense of lengthening the pulse sequence. A different T_1 contrast in the images also results. The T_R used here was convenient both for the (large) contrast of T_1 between the uninvaded and invaded rock and for the timescale of the process examined. Through Figures 3b to 3e ($t = 9.5$ s to $t = 15.2$ s), a

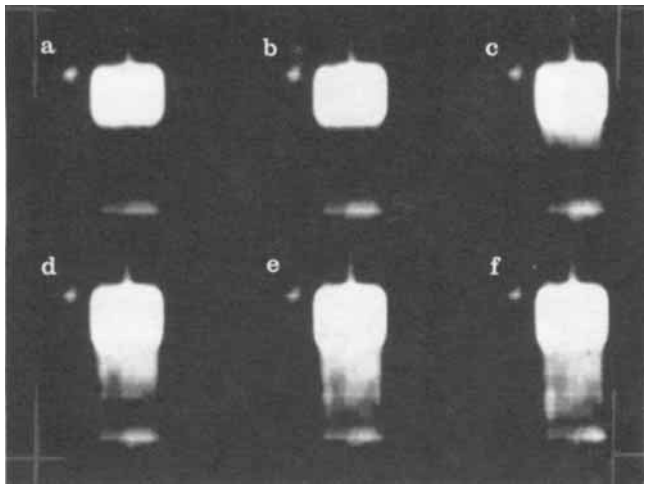

Figure 3. Sequence of "prefocused FLASH" images of the pressure cell during the depth filtration, taken from the full sequence of 64 frames recorded.

Acquisition time for each frame was 1.9 s, with a T_R of 29 ms for each acquisition of Figure 1. Frames (a) to (f) started at t = 7.6 s, 9.5 s, 11.4 s, 13.3 s, 15.2 s, and 119.7 s, respectively, after the experiment start (t = 0). Slice thickness was 1.0 cm and images are 128 pixels (horizontal, frequency-encoded) by 64 (vertical, phase-encoded). Linear interpolation has been applied. Pulse length was 5 ms with a slice gradient of 4.5 mT·m^{-1}. Read gradient was 22 mT·m^{-1} and maximum phase encode gradient was 20 mT·m^{-1}. The gradient recalled echo time T_G was 1.1 ms. The spot at the upper left arises from a drop of clay suspension exterior to the pressure cell.

progressive invasion front of clay-bearing fluid is seen because of its influence on the T_1 of the pore fluid. In this example, the displacement appears to be piston-like and stable at the spatial resolution available here, although we have observed other cases where fingering can be seen, either around apparent heterogeneities or as leakage past the rubber collar (Figure 4). The front velocity appears to be nearly steady until $t = 15.2$ s (Figure 3e), when the progression abruptly stops (compare $t = 119.7$ s, Figure 3f, just short of the end of the specimen. This behavior is confirmed on repeated trials, the depth reached by the front varying from specimen to specimen; and the case reported here is intermediate for this stone and suspension.

Image intensity is also subject to bias by changes in T_2^*, as well as changes in T_1 (Eq. 1). The T_2^* bias is in the opposite sense to the T_1 bias: that is, an increase in image intensity over time may logically be interpreted as either a reduction in T_1 or an increase in T_2^*. However, although clay particle invasion may be expected to reduce both T_1 and T_2^*, it is not physically plausible that it should increase T_2^*. Our primary qualitative interpretation, which is that increases in image intensity over time represent reductions in T_1, is therefore robust even in the presence of accompanying reductions in T_2^*. The effect of the latter is simply some attenuation of the intensity enhancement caused by the T_1 reduction. The further logical possibility of an *increase* in proton density may be safely dismissed in the present context; and it is not possible that invasion by solid particulates should increase the rock's porosity.

Full quantification of reductions in T_1 and T_2^* in terms of

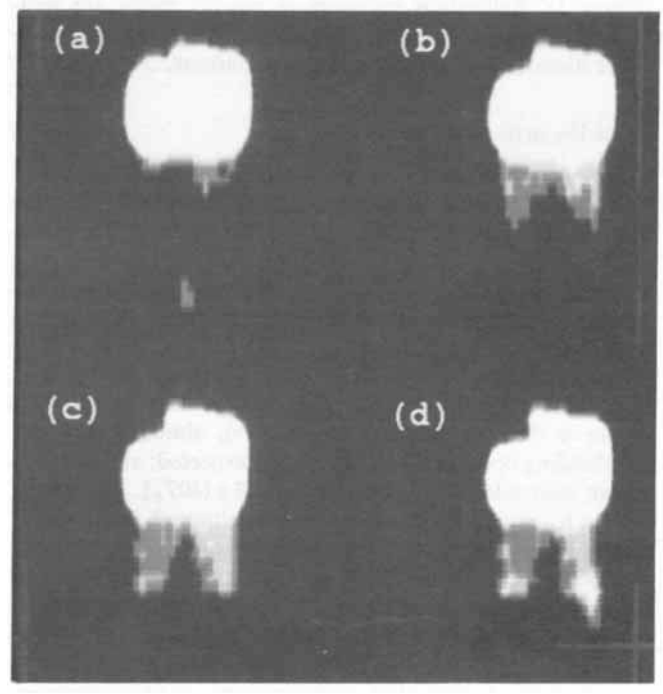

Figure 4. Nonuniform invasion.

Frames (a) to (d) started at t = 9.5 s, 11.4 s, 13.3 s, and 119.7 s, respectively, after the experiment start. Other imaging parameters as for Figure 3.

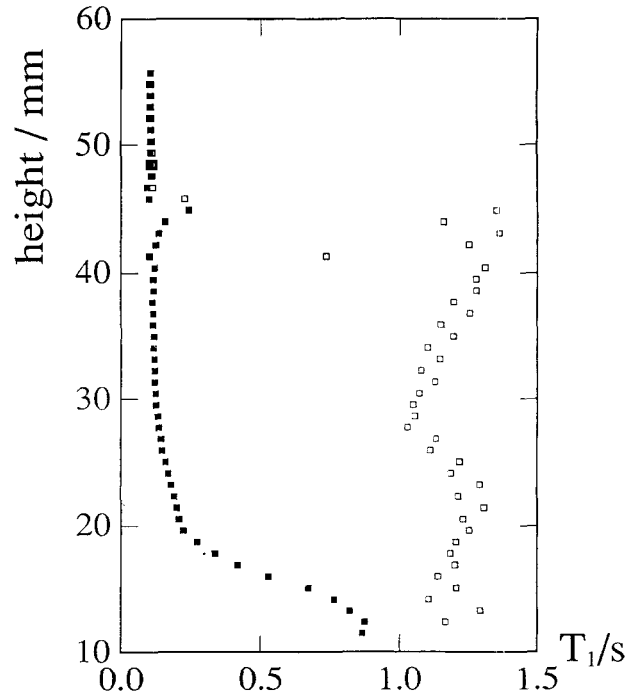

Figure 5. Profiles of relaxation time T_1 through the height of the cell obtained by the inversion-recovery method combined with one-dimensional spin-echo imaging.

Open symbols, before filtration; solid symbols, after; corresponding to Figures 2a and 2b. Seventeen recovery times quasilogarithmically spaced between 0.5 ms and 8 s were used, with 8 s relaxation delay between acquisitions, and 4 signal averages with phase cycling giving a data acquisition time for the sequence of about 15 minutes. Composite inverting pulses were used to counter the effect of rf field inhomogeneity near the resonator ends. Data points from the frit have been eliminated. The rock-mud interface is at 46 mm height. Gradient strength was 13 mT·m^{-1}.

clay content would be a more involved task, which we have not yet attempted. However, the predominantly T_1-weighted interpretation of Figure 3 is confirmed by the data of Figure 5, showing profiles of T_1 through the entire specimen, before and after the filtration. The method of Horsfield et al. (1989) was used. Figure 5a shows a long T_1 (~ 1.2 s) in the uninvaded rock, below a suspension of $T_1 \sim 100$ ms. Heterogeneity (probably local variations in mean pore size) in the rock is apparent through the variation in T_1 in the uninvaded rock. After the filtration (Figure 5b), the rock T_1 has fallen to near the suspension value, with a steep recovery to about 0.9 s at about the position of the front seen in Figures 3e and 3f.

Discussion

The profiles of Figure 5 are qualitatively consistent with data (to be reported in detail elsewhere) on other rocks and mud types, which we have obtained by the method of Horsfield et al. (1989). A rapid change in profile was observed within the first 15 minutes of filtration, followed by little further change within the rock on a period of 12 hours. On such *long* timescales, an external filter cake develops and is easily imaged (Horsfield et al., 1989). Such data and the new results reported here are consistent with the ubiquitous observation of a "spurt" of filtrate when filtration processes are observed using extended filter media like sedimentary rocks (Darley, 1965), followed further by much slower loss of filtrate according to the $t^{1/2}$ law of cake filtration kinetics (Philip and Smiles, 1982). However, for cake filtration to start, where the particle to pore size ratio is much less than one, as here, some initial clogging of the medium must take place.

We believe that the images reported here provide the first direct observations of such particle-clogging dynamics, revealing not only the timescale of the clogging process [previously available only from detailed studies of filtrate outflow (Darley, 1965)], but also its spatial extent and distribution. The most significant qualitative observation from our images is thus that the clay invasion does indeed eventually *stop*, and quite suddenly.

For this demonstration, we deliberately chose a medium of extreme permeability and pore size, with particle penetration depth expected to be large, but it would appear that it forms a suitable model system for the systematic study of such processes, which are of immediate interest in the mechanics of oil-well drilling. In drilling, cutting prevents the formation of an exterior filter cake, but an interior clogging zone (continuously cut away and reforming) significantly restricts filtrate flow from borehole fluids into the rock. The consequent influence on pore pressure fields around the bit strongly influences drilling performance (Peltier and Atkinson, 1987; Fordham et al., 1991).

Some remarks on the limits of the technique are in order. For processes known to be essentially one-dimensional, two-dimensional images are unnecessary; a single profile suffices, and NMR imaging is capable of profile generation very rapidly. The sequence of Figure 1 can then be shortened to an acquisition time of only 29 ms per profile. This time saving can then be used to observe even more rapid phenomena (in 1-D) or to employ variable recovery times to expand the range of T_1-contrast in what amounts to a modified saturation-recovery determination of the T_1 profile. It is then unnecessary to have prior knowledge of the T_1 contrast to determine a suitable T_R. The limitation to specimens of sufficiently long T_2^* is a severe one for many reservoir rocks; however, an obvious variant (with some sacrifice of speed) would be to use 180° refocusing pulses as in normal spin-echo imaging. The method then applies to media of sufficiently long T_2, and most porous media exhibit $T_2 > T_2^*$ at the magnetic field strengths (about 2 tesla) used in our imaging systems.

Acknowledgment

We thank Dr. Herchel Smith for a munificent endowment (L.D.H. and T.A.C.) and research studentship (T.P.L.R.) and M. A. Horsfield for stimulating discussions. E.J.F. thanks the S.E.R.C. (United Kingdom) and the Royal Society for the award of an Industrial Fellowship and Schlumberger for leave of absence.

Literature Cited

Darley, H. C. H., "Designing Fast Drilling Fluids," *J. Petrol. Tech.*, 465 (1965).

Edelstein, W. A., J. M. S. Hutchison, G. Johnson, and T. Redpath, "Spin-Warp NMR Imaging and Application to Human Whole-Body Imaging," *Phys. Med. Biol.*, **25**(4), 751 (1980).

Fordham, E. J., P. S. Hammond, H. K. J. Ladva, L. Schwartz, and D. Wilkinson, "Early Stages of Drilling Mud Filtration on Permeable Rock," *Physics and Chemistry of Colloids and Interfaces in Oil Production*, J. Lecourtier and H. Toulhoat, eds., Editions Technip, Paris, in press (1992).

Frahm, J., W. Hänicke, and K.-D. Merboldt, "Transverse Coherence in Rapid FLASH NMR Imaging," *J. Magn. Reson.*, **72**, 307 (1987).

Fripiat, J., J. Cases, M. François, and M. Letellier, "Thermodynamic and Microdynamic Behavior of Water in Clay Suspensions and Gels," *J. Coll. Interf. Sci.*, **89**(2), 378 (1982).

Haase, A., J. Frahm, D. Matthaei, W. Hänicke, and K.-D. Merboldt, "FLASH Imaging: Rapid NMR Imaging Using Low Flip-Angle Pulses," *J. Magn. Reson.*, **67**, 258 (1986).

Hall, L. D., T. A. Carpenter, and T. P. L. Roberts, "MRI Involving Pulse Annealing," U.K. Patent No. 9007655.5 (1990).

Hall, L. D., T. Marcus, C. Neale, B. Powell, J. Sallos, and S. L. Talagala, "Design of Volume Resonator Probes for NMR Imaging," *J. Magn. Reson.*, **62**, 525 (1985).

Horsfield, M. A., E. J. Fordham, C. Hall, and L. D. Hall, "^{1}H NMR Imaging Studies of Filtration in Colloidal Suspensions," *J. Magn. Reson.*, **81**, 593 (1989).

Kirkpatrick, S., C. D., Gelatt, Jr., and M. P. Vecchi, "Optimisation by Simulated Annealing," *Sci.*, **220**, 671 (1983).

Leary, E., *The Building Limestones of the British Isles*, p. 41. H.M.S.O., London (1983).

Morris, P. G., *N.M.R. Imaging in Medicine and Biology*, Chap. 4, O.U.P. (1986).

Peltier, B., and C. Atkinson, "Dynamic Pore Pressure Ahead of the Bit," *S.P.E. Drilling Eng.*, **2**, 351 (1987).

Philip, J. R., and D. E. Smiles, "Macroscopic Analysis of the Behaviour of Colloidal Suspensions," *Adv. Coll. Interf. Sci.*, **17**, 83 (1982).

Roberts, T. P. L., T. A. Carpenter, and L. D. Hall, "Design and Application of Prefocused Pulses by Simulated Annealing," *J. Magn. Reson.*, **89**, 595 (1990).

Roberts, T. P. L., T. A. Carpenter, and L. D. Hall, "Elimination of Steady-State Magnetization in Fast Gradient-Recalled Echo Imaging by the Use of Prefocused Pulses," *J. Magn. Reson.*, **91**, 204 (1991).

Manuscript received July 10, 1991, and revision received Oct. 21, 1991.